Microstructure and cavitation erosion performance of nickel-Inconel 718 composite coatings produced with cold spray

Marios Kazasidis, Shuo Yin, Jonathan Cassidy, Tatjana Volkov-Husović, Milica Vlahović, Sanja Martinović, Kyriakopoulou Elena, Rocco Lupoi

PII: S0257-8972(19)31185-5

DOI: https://doi.org/10.1016/j.surfcoat.2019.125195

Reference: SCT 125195

To appear in: *Surface & Coatings Technology*

Received date: 23 September 2019

Revised date: 11 November 2019

Accepted date: 25 November 2019

Please cite this article as: M. Kazasidis, S. Yin, J. Cassidy, et al., Microstructure and cavitation erosion performance of nickel-Inconel 718 composite coatings produced with cold spray, *Surface & Coatings Technology* (2019), https://doi.org/10.1016/j.surfcoat.2019.125195

Microstructure and cavitation erosion performance of nickel-Inconel 718 composite coatings produced with cold spray

Marios Kazasidis[a], Shuo Yin[a], Jonathan Cassidy[a], Tatjana Volkov-Husović[b], Milica Vlahović[c], Sanja Martinović[c], Kyriakopoulou Elena[d], Rocco Lupoi[a]

[a] Trinity College Dublin, The University of Dublin, Department of Mechanical and Manufacturing Engineering, Parsons Building, Dublin 2, Ireland

[b] University of Belgrade, Faculty of Technology and Metallurgy, 4 Karnegijeva St, 11000 Belgrade, Serbia

[c] University of Belgrade, Institute of Chemistry, Technology and Metallurgy, 12 Njegoševa St, 11000 Belgrade, Serbia

[d] Shipbuilding Technology Laboratory, School of Naval Architecture and Marine Engineering, National Technical University of Athens, 9 Heroon Polytechniou st., Zografos, Athens, Greece

kazaside@tcd.ie

Keywords: cold spray, nickel, Inconel 718, cavitation erosion, coating

Abstract

The cold spray technique was employed in this study to produce pure nickel (Ni) and nickel-Inconel 718 powder deposits on duplex stainless steel substrates. High quality coatings were manufactured using nitrogen as the propellant gas. The coatings exhibited satisfactory Inconel 718 (In718) retention within the Ni matrix due to the highly ductile binder phase necessary for fabrication. The characterization of the coating microstructures was implemented by means of X-ray diffraction, electron microscopy, energy-dispersive X-ray spectroscopy, and microhardness testing. In addition, the erosion resistance of both coatings was evaluated by performing cavitation erosion tests, with the analysis of the eroded surfaces revealing different erosion mechanisms for each coating. The results demonstrated the efficiency of the cold spray technique for use in the production of metal-metal matrix composite coatings and the potential of In718 use in applications which demand enhanced cavitation erosion resistance.

1. Introduction

Cavitation erosion is a critical problem[1,2] which is commonly encountered in hydraulic systems such as turbine blades, valves, propellers, and pipelines. It is typically caused by a rapid drop in the fluid pressure and the subsequent generation of steam bubbles which collapse on the metal surface[3] of the machinery. The energy released during this phenomenon can lead to local plastic deformation of the material and mass removal, while its extended action can result in malfunction or even failure of the component[3]. Conventional approaches for the mitigation of cavitation erosion include the use of high velocity oxy-fuel, thermal and plasma spraying for cermet deposition, or surface techniques such as boronizing and cladding[4].

The cold spray technique has been extensively used in recent decades for the fabrication of coatings, with the aim of enhancing the surface properties of metallic materials, decelerating the mass loss rates, extending the lifespan of metallic components, and reducing the production costs[5]. Its advantages include the elimination or restraint of undesirable

metallurgical phenomena that can be met in other thermal spraying techniques[6] such as phase transformation, grain growth, and oxidation[7]. Further benefits emerge from its high deposition efficiency and the high hardness of the coatings which can be useful in certain applications[8]. In addition, the cold spray technique has been proven as an efficient technique for the fabrication of metal matrix composites[9–12] (MMCs), focusing on the use of ceramic refractory particles such as tungsten carbide (WC)[6] and aluminium oxide (Al_2O_3)[13] for the production of cermets. In most investigations, a ductile material such as aluminum[11,14], nickel[10,15] or copper[16], comprise the metallic binder phase. In order to achieve high quality coatings, there are many processing parameters, such as spraying temperature and pressure, which must be accounted for during the cold spray technique. However, when used to produce metal matrix[11,17] composites, there are additional processing parameters which must be considered. These include the percentages of the powders in the feedstock, and their differences in terms of particle size distribution and particle density.

The current research trend has been primarily focused on cermets, however, some investigations deal with the fabrication of metal-metal matrix composites using the cold spray technique. Shin et al.[18] sprayed a W- 30 wt. % Cu original feedstock with the aim of maintaining the same ratio in the final coating with the proper adjustment of the particle size distribution and the preheating temperature of the gas. Yu et al.[19] scrutinized the anode corrosion performance of a ternary composite composed of Al5056 and In718 reinforcement alloys within a pure aluminium matrix. More recently, Shuo et al.[20] investigated the cold spray coating of a composite powder consisting of a diamond core, and consecutive layers of Ni (inner) and Cu (outer).

Ni based superalloys have been widely used in recent years for the production of cold sprayed coatings due to their enhanced mechanical properties, especially at high temperatures[21–23]. It is for this reason that they are used in a series of severe service applications[24] including turbine discs, high-pressure compressors[1], and nuclear reactors. However, the deposition of Ni-based superalloys such as In718 using the cold spray technique is restricted due to three basic reasons. Firstly, there is a high risk of nozzle clogging[21] which results from the high nozzle wall temperature[25] and the high critical velocity of superalloys[22]. Secondly, the high cost of He[8] (which is approximately ten times higher than nitrogen[26]). It is generally stated that He is strongly proposed[27] as a propellant gas for the fabrication of high-quality coatings as it generates high gas velocities and thus high particle impact velocities. Using N_2 instead results in high porosity[28] and/or low coating thickness due to its limited gas acceleration capability[8]. For instance, Pontarollo et al. cold sprayed Inconel 625 on 316L stainless steel with nitrogen. The fabricated coatings had a porosity range from about 3 to 5% and a thickness from 60 to 480 μm. In addition, Levasseur et al.[29] cold sprayed In718 onto a mild steel substrate using nitrogen as the propellant gas with a pressure of 35 bar and preheating temperature of 800 ^{o}C. The resultant coatings exhibited porosity values of 3% and poor mechanical properties in the as sprayed condition. Furthermore, Ma et al.[30] found that the porosity of cold sprayed In718 produced with He was 0.21%, which is much less than the 1.84% lowest porosity value achievable with nitrogen. Thirdly, in the case of the cold spraying of superalloys, their high hardness can result in the erosion of the interior nozzle surface as well as the deposition of the erosion products such as impurities into the coating[31].

In the present study, In718 nickel superalloy was used as a reinforcement material within the ductile pure Ni matrix for cold spray. The high strength and fracture toughness of this alloy in extreme conditions arises from two major strengthening mechanisms. Firstly, the solid solution strengthening of its Ni rich gamma austenitic matrix with chromium[32,33] as the substitutional alloy element. Secondly, the precipitation hardening[34] with a uniform dispersion of intermetallic phases and more specifically the face centered cubic $\gamma'(Ni_3(Ti,Al))$

which attains a cubic or spherical shape, and the body centered tetragonal γ´´ (Ni_3Nb) which is a coherent metastable phase with a disk shape morphology. The aforementioned precipitates significantly contribute to the preservation of material properties at elevated temperatures[35], by hindering the movement of dislocations[36]. In addition the existence of the stable orthorhombic delta δ (Ni_3Nb) phase[37], eta[38] η hexagonal ordered (Ni_3Ti), sigma[38] (σ) phase, Laves phase[32,39], carbides and carbonitrides[40] as constituents of In718 has been reported depending on the heat treated condition. Moreover, several researcher have investigated their effects on the microstructure[41,42], mechanical properties[40] and corrosion performance[43] of the alloy.

In this study, the authors aimed to use the cold spray technique with high pressure for the manufacturing of the composite coating in order to achieve the enhancement of Ni coating erosion properties and the avoidance of helium use for the deposition of In718. The innovative character of the work lies on both the fabrication of a newly developed material with advanced properties and the essential reduction in process costs. The produced cold sprayed coatings were studied in terms of microstructure and cavitation erosion in order to investigate their potential use in relative applications.

2. Experimental methodology

2.1 Materials

Spherical Ni (-45/+16 μm, Praxair) and In718 (-45/+15 μm, LPW) were used as the powder feedstock in this work. The two powders were mechanically blended at equivalent volume ratios prior to spraying. Stainless steel 2205 cylindrical specimens with dimensions of 12 mm height and 30 mm diameter were used as the substrate material.

The chemical composition of the In718 powder was determined using Inductively Coupled Plasma Mass Spectrometry (ICP-MS) in conjunction with Inert Gas Fusion (IGF) methods (see table 1).

Table 1. The chemical composition of the In718 powder (wt.%)

Al	B	C	Ca	Co	Cr	Cu	Fe	Mg	O
0.5	0.001	0.04	<0.01	0.07	18.99	<0.1	Bal	<0.01	0.02
Mn	Mo	Nb+Ta	Ni	P	S	Se	Si	Ti	N
0.01	3.0	5.06	53.08	<0.005	0.002	<0.001	0.05	0.92	0.01

2.2 Cold spraying process

The feedstock powders were deposited using an in-house cold spray system (Trinity College Dublin, Ireland) as illustrated in Fig. 1a. Nitrogen was used as the propellant gas at a pressure of 3.0 MPa and preheating temperature of 900 ^{o}C. The powders were fed into the system from a powder hopper (PF100WL, Uniquecoat Technologies LLC, USA) with a feed rate of 210 and 234 g/min for the Ni and the Ni-In718 respectively. The powders were accelerated towards the substrate through a WC-Co de Laval nozzle with a divergent length of 180 mm, throat diameter of 2 mm and outlet diameter of 6 mm.

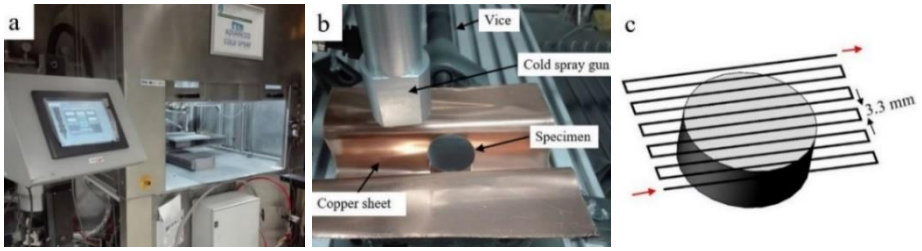

Fig. 1. (a) The used Cold Spray system, (b) positioning of the billets before the cold spray process, (c) the selected zig-zag strategy.

The specimens were clamped on a vice, with the area adjacent to the substrate suitably protected from overspray by shielding with a sacrificial copper sheet as depicted in Fig. 1b. The movement of the nozzle was controlled by a computer numeric control system. The nozzle standoff distance and traversal speed was set at 30 mm and 25 mm/s, respectively. A two-pass building strategy with a zig-zag pattern was programmed in G-code as presented in Fig. 1c where the red arrows indicate the nozzle movement direction. At the end of the cold spraying process, the final thickness of the coating reached approximately 3 mm.

2.3 Materials characterization

The particle size distribution of the feedstock powders was analyzed using a Horiba LA-920 laser scattering particle analyzer (ENBIO, Ireland). Macrotexture and phase composition analysis was implemented using a MXP18 X-ray diffractometer (XRD, Bruker, USA) with Cu Kα radiation. The step size was set at 0.03^o and the time per step was 10 seconds, while the scan was performed at an angular range from 30^o to 110^o. Powders and coatings were mounted into a conductive resin and subsequently subjected to grinding and polishing by using standard metallographic techniques for microstructure observation. The polished cross-sections were then observed with scanning electron microscope (SEM, Carl Zeiss UTRA, CRANN). Etching was performed with Marbles reagent (50 mL HCl, 10 gr $CuSO_4$ 50 mL H_2O) in order to reveal the microstructure of the coatings as proposed by ASTM E407[44].

Image J analysis software was used for the estimation of the flattening ratio (FR) which is defined as the ratio of the long axis to the short axis of a flattened particle. Thirty particles were measured in each case and used to calculate an average value. The same software was also used for calculating the average content of In718 in the composite coatings based on five optical micrographs. In718 recovery was also measured using energy dispersive X-ray spectroscopy (EDX), based on the iron and chromium content of In718 powder and Ni-In718 coating. Three EDX spectra were obtained for each case.

The microhardness of both the substrate and the manufactured coatings was evaluated using a Vickers microhardness tester (Mitutoyo MVK-H1, Japan) by applying a load of 300 g with a dwell time of 10 s. Ten repetitions were executed for each sample to calculate the average value.

2.4 Cavitation Erosion testing

The cavitation erosion tests were implemented using a vibratory apparatus as presented in Fig. 2a, b according to the ASTM G32[45]. The experimental set-up consisted of a 360 W generator of high frequency, an electrostrictive transducer, a mechanical vibration transformer and a bath of distilled water where the cold sprayed samples were placed.

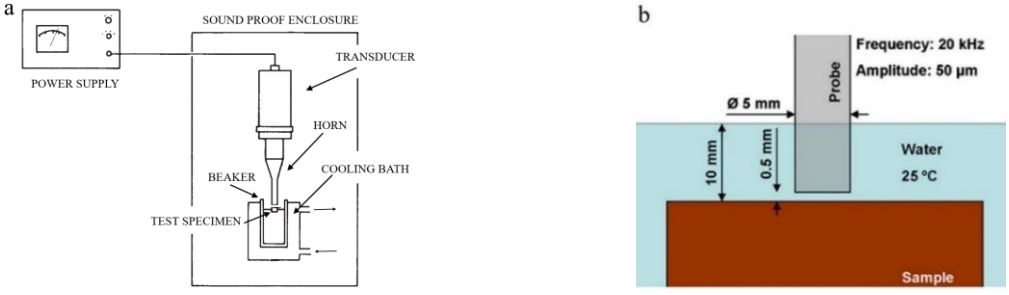

Fig. 2. (a) Schematic representation of the cavitation erosion test set-up (modified from ASTM G32), (b) experimental details of the cavitation erosion experiment.

The frequency of the vibrations was set at 20 kHz and their amplitude at the top of the ultrasonic transformer at 50 μm. The gap between the surface of the cold spray coating and the transformer probe was 0.5 mm.

Before the cavitation erosion test, the coatings' surfaces were grinded with silicon carbide disks up to 4000 grit, and polished with 3 μm alumina suspension in order to attain equivalent roughnesses. The mass loss and the degradation level were measured during the testing at preselected time intervals i.e. 30, 60, 90, 120, 150, 180, and 240 minutes. A weighing scale with 0.1 mg resolution was used to record the mass loss versus time. Prior to each measurement, the samples were cleaned with ethanol and dried with compressed air. On the eroded surfaces, the degradation level was calculated by dividing the total eroded area (P), as measured using a stereomicroscope (Leica L2, Germany), by the area of the probe (P_o) which has a diameter of 16 mm. A final evaluation of the erosion characteristics was employed by means of stereo and scanning electron microscopy.

3. Results and Discussion

3.1 Materials Characterization

The gas atomized powders used in this study are presented in Fig. 3. In most cases, they attain a spherical shape (Fig. 3 a, b), however, in nickel powder some satellites, agglomerations and irregular shapes are evident. The powder particles are almost free from pores (Fig. 3 b, d) as their porosities were estimated in the order of 0.02% and 0.06% for Ni and In718 respectively.

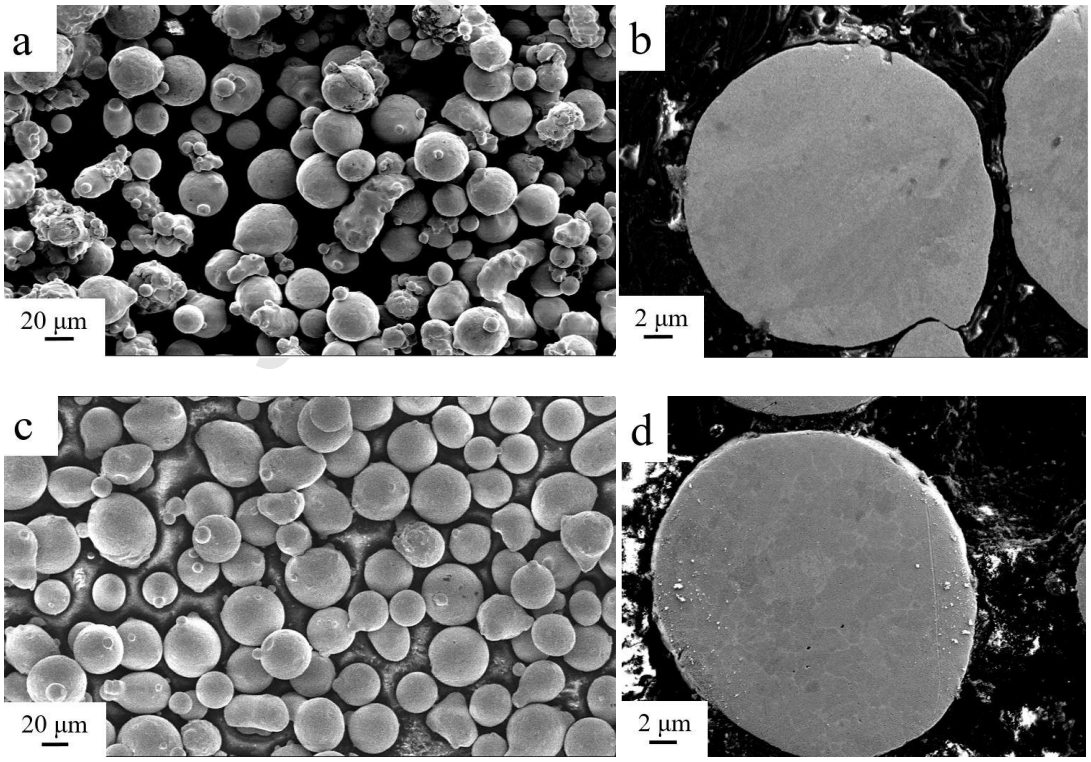

Fig. 3. Morphology of the powders used in this study: (a) Ni powder overall view, (b) as polished Ni powder cross-section, (c) In718 powder overall view, (d) as polished In718 powder cross-section.

The particle size distributions of the powders are depicted in Fig. 4. In the case of Ni, the mean and median size of the distribution were calculated at 29.1 μm and 27.7 μm respectively. The corresponding values for the In718 powder were 33.9 μm and 34.6 μm. It can therefore be stated that the In718 powder employed in this study, had on average, a slightly larger diameter in the order of +14%, compared to the Ni powder.

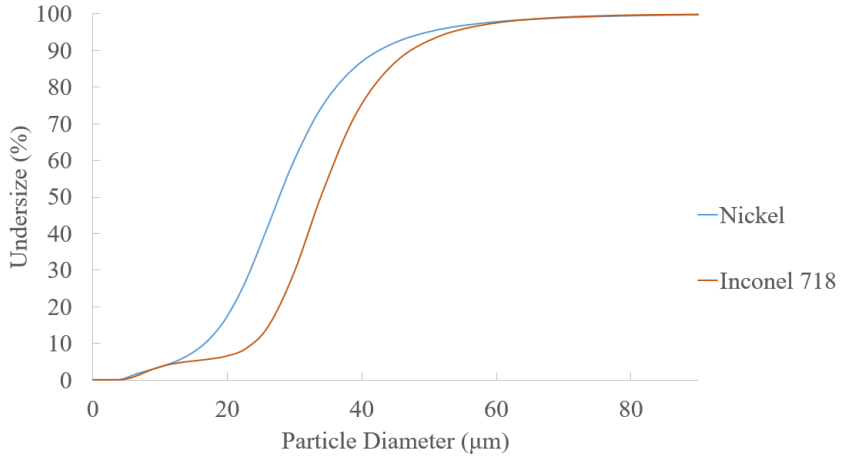

Fig. 4. The particle size distribution of the Ni and In718 powders.

As far as the substrate is concerned, it attains a dual phase microstructure with the coexistence of the ferrite and austenite at equal percentages. Its hardness was estimated at about 268 HV.

3.2 Microstructural characterization of coatings

3.2.1 Microstructural features

The XRD spectra were classified into two different categories according to the expected obtained phases: (a) and (b) for the pure Ni powder and coating respectively, and (c) and (d) for the composite powder and coating. The results are depicted in Fig. 5. As expected, in the case of Ni and Ni coating, the typical face centered cubic (FCC) γ-austenite was detected exhibiting strong peaks. In the mixed powder and the composite coating, the γ peaks may theoretically[46] overlap with those of γ´ and γ". As a result, the existence of the two latters can be assumed but without definite evidence[32].

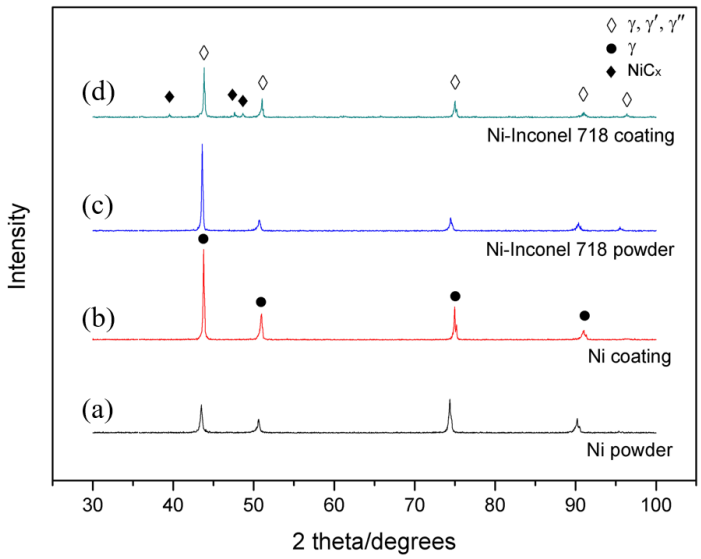

Fig. 5. The obtained XRD spectra of the powders and the cold sprayed coatings.

In contrast to the feedstock powder (Fig. 5c), the composite coating exhibited low peaks (Fig. 5d) which are representative of nickel carbides. This may be attributed[47,48] to carbide coarsening due to the high temperature of the cold spray process (900 ^{o}C). In addition, the coatings' spectra presents a slight displacement at certain peaks to higher angles (in the order of 0.5 degrees), a phenomenon that can be correlated to the development of an intense residual stress field during the cold spray process and the resulted distortion of the crystal lattice due to the plastic deformation[49] as has been also reported by Wolfe et al.[50].

The cross-sectional SEM images of the Ni and Ni-In718 coatings are presented in Fig. 6. The interface between the coating and substrate in both cases is indicated by the white arrows (Fig. 6a, b). The Ni coating showed an intimate contact with the substrate and porosity value of 0.5% (Fig. 6c). The interface between the stainless steel substrate and the composite coating exhibits a slight flaw (red dotted circle in Fig. 6b), which implies lower bond strength. The porosity of the Ni-In718 coating was measured at 1.8% (Fig. 6d). It can therefore be stated that 50 vol. % In718 addition into Ni resulted in an increment of porosity by more than three times. However, the overall porosity of the sample remains at low levels.

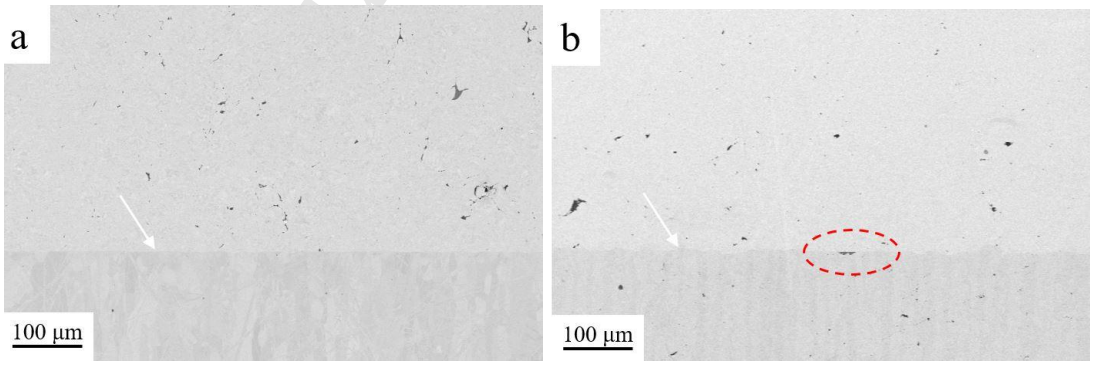

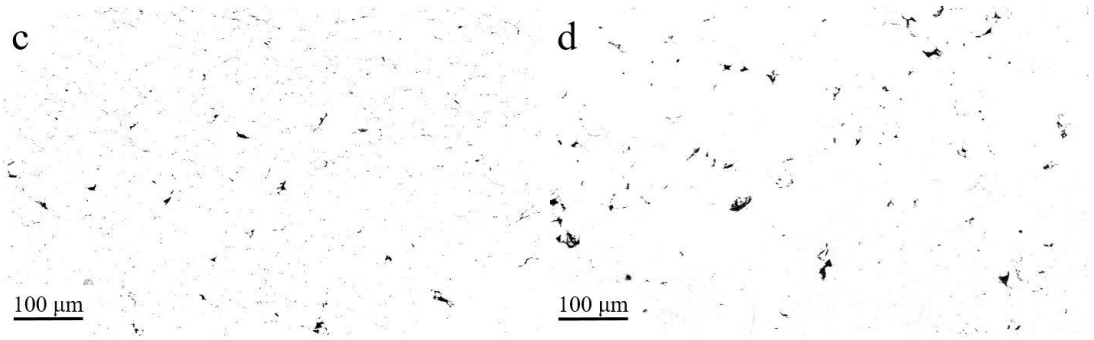

Fig. 6. Images of the as polished cold sprayed sample: (a) interface of Ni coating, (b) interface of Ni-In718 coating, (c) porosity of Ni coating, (d) porosity of Ni-In718 coating.

The microstructural features of the coatings were revealed upon completion of the etching process. In this way, the distinction between the Ni matrix and the In718 reinforcement was achieved as depicted in Fig. 7. The corresponding EDX line scan indicates qualitatively the trend of the three basic alloying elements (Ni, Fe, Cr) as the measurement point moves from an In718 to a pure Ni particle. As expected, the percentage of Ni present increases at the expense of Fe and Cr.

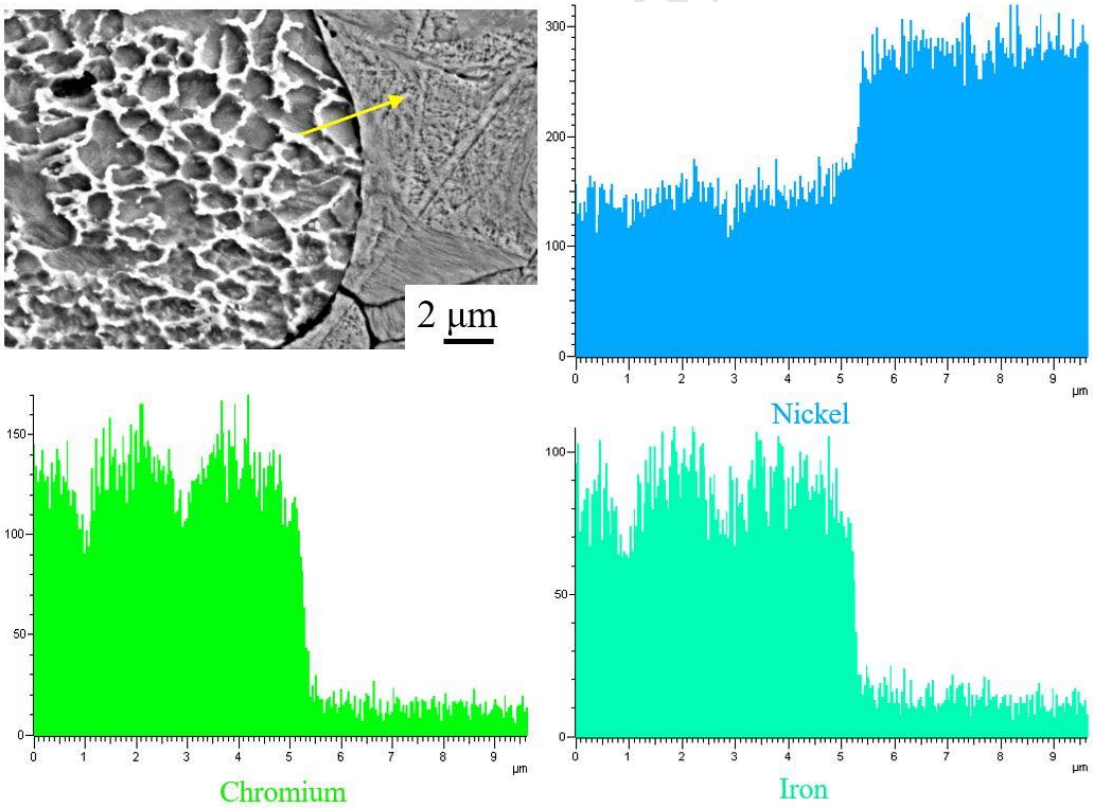

Fig. 7. EDX line scan perpendicular to the interparticle boundary between In718 and Ni.

Fig. 8 shows the etched cross-section of the coatings as observed by SEM. In most areas of Ni coating (Fig. 8a) the etching is more intense at the interparticle boundaries compared to the grains at the interior of the particles which indicates that these areas attain the weakest regions inside the cold spray coating. The dispersion of In718 particles presents a high level of uniformity and consistency inside the Ni matrix (Fig. 8b). The internal defects of the coating are mainly presented at the interface between In718-In718 and In718-Ni particles. Interparticle pores and poor interparticle bonding (red arrows in Fig. 8b) are related with the

presence of In718 particles, which undergo minor plastic deformation compared to the Ni, due to their higher yield strength. Luo et al.[51], dealt with this issue by spraying In718 under moderate conditions (2.5 MPa, 700 ^{o}C) using nitrogen as the propellant gas. The enhancement of the particle deformation was achieved by using large sized 410 stainless steel particles and in-situ forging, leading to a reduction in the porosity level from 5 vol. %, down to 0.17 vol. %.

The plastic deformation that is exhibited by the In718 particles is predominantly close to the periphery of the particles as presented in Fig. 8c. However, some particles preserve an intact morphology as can be seen in Fig. 8d where the formation of pores was not observed due to the extremely high deformation of the surrounding Ni particles.

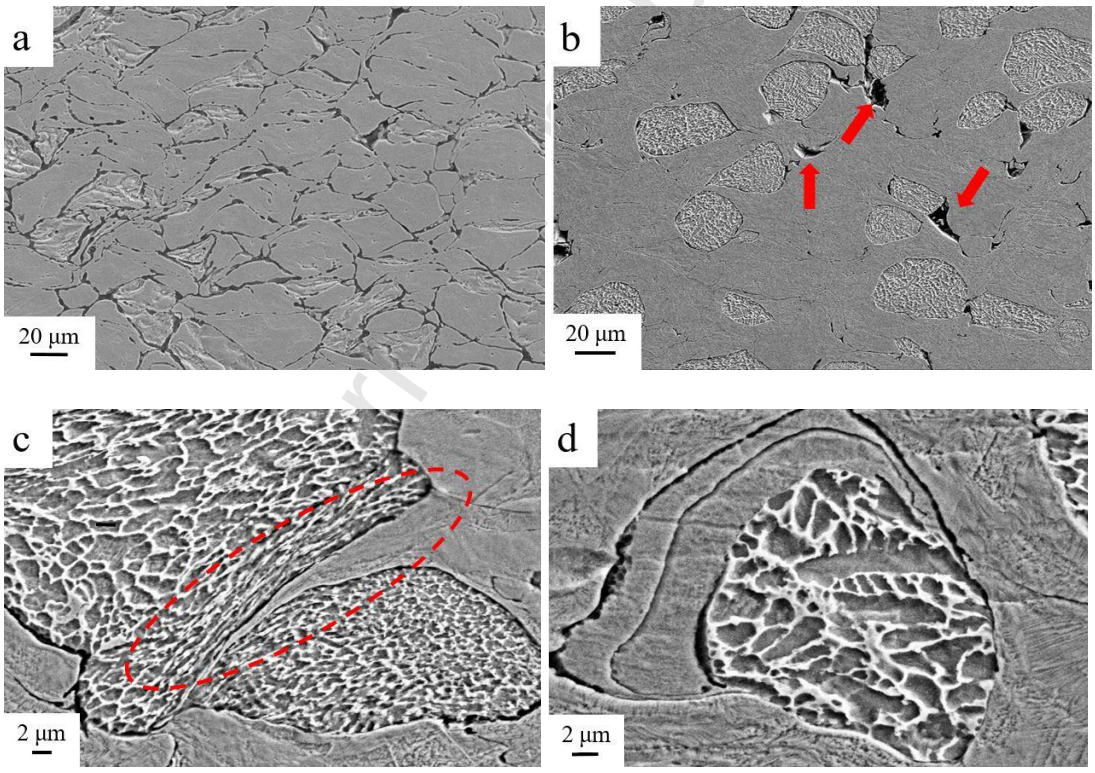

Fig. 8. Cross-sectional images of the etched cold sprayed coatings: (a) Pure Ni coating, (b), (c), (d) Composite coating.

3.2.2 Coating composition and microhardness

It was found that approximately 20 vol. % of In718 was retained in the composite coating with the use of binary images generated by Image J software as indicatively presented in Fig. 9a. The respective percentage as estimated with energy dispersive X-ray spectroscopy was marginally higher, at 25 vol. % (see indicatively Fig. 9b and c).

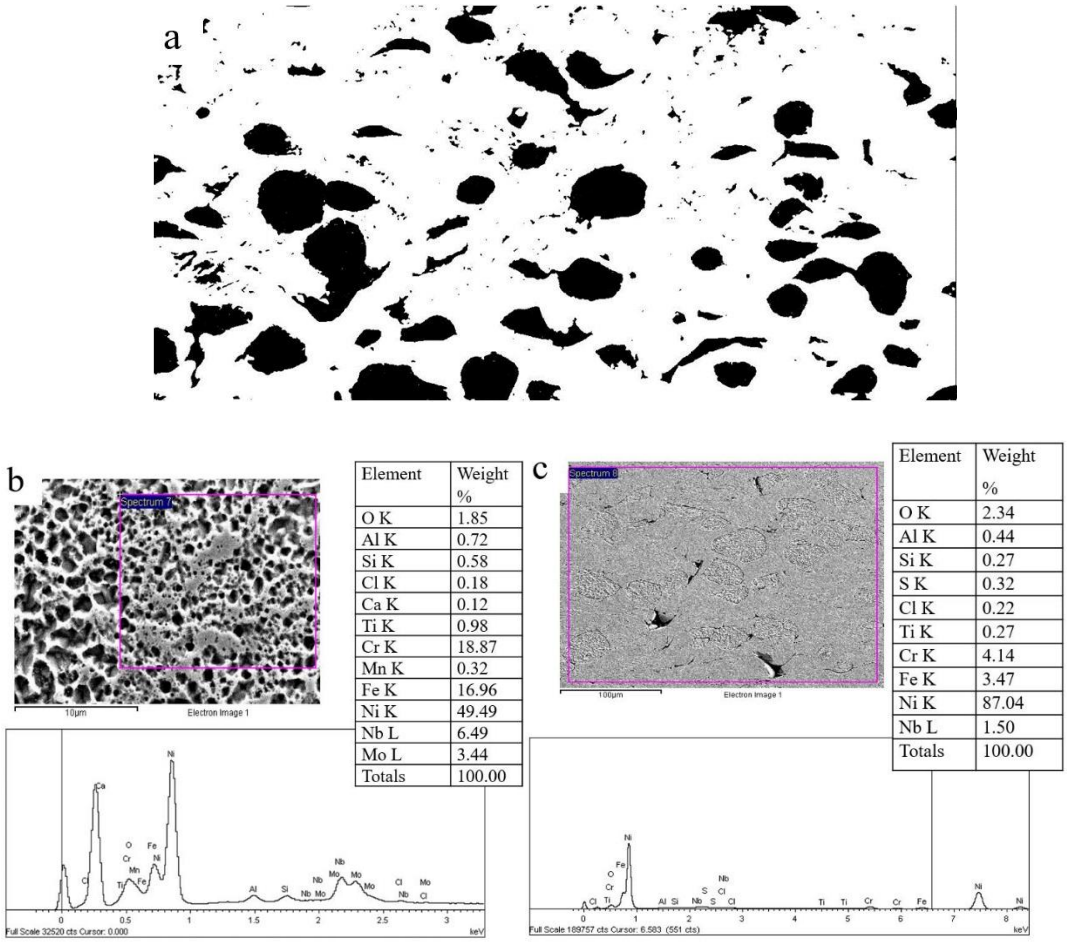

Element	Weight %
O K	1.85
Al K	0.72
Si K	0.58
Cl K	0.18
Ca K	0.12
Ti K	0.98
Cr K	18.87
Mn K	0.32
Fe K	16.96
Ni K	49.49
Nb L	6.49
Mo L	3.44
Totals	100.00

Element	Weight %
O K	2.34
Al K	0.44
Si K	0.27
S K	0.32
Cl K	0.22
Ti K	0.27
Cr K	4.14
Fe K	3.47
Ni K	87.04
Nb L	1.50
Totals	100.00

Fig. 9. (a) Binary image of the In718 dispersion (black areas) inside the Ni matrix (white areas), (b) EDX spectrum of In718 particle, (c) EDX spectrum of the composite coating.

It can be deduced that 40-50% of the In718 powder feedstock was successfully deposited, which is less than what has been reported in relevant studies of metal-metal matrix composites, mainly due to the moderate ductility of In718. For instance, Al-Mangour et al.[52] achieved a 70-90 vol. % retention of the ductile L605 powder in a stainless steel 316L matrix. Additional considerations on this issue should involve not only the ability of the material to deform, but also the size of the particles, a factor that significantly affects their kinetic energy. Novoselova et al.[53], mention the higher retention of titanium at the expense of aluminium in Ti-Al composite, resulted from the deceleration of Al particles due to the bow shock phenomenon. However, the extremely high porosity of the coating (in the order of 20%) should further highlight the importance of plastic deformation which has to be achieved either through the selection of ductile metals and/or the increment of particle velocity within the window of deposition for the specific system.

As compared to the metal matrix coatings reinforced with ceramic particles[10], In718 appears to exhibit a higher recovery in the final coating due to the metallurgical bonding which can be formed at the metallic interface between ductile metallic materials. On the contrary, it is considered that ceramic particles can be embedded within the metal matrix, without any chemical interaction present[20].

The results of microhardness testing are presented in Fig. 10a. In718 addition into the Ni matrix resulted in an increase of the average microhardness in the order of +17%, a commensurate percentage to the In718 retention into the composite coating. Fig. 10b depicts the estimated FRs of Ni and In718 particles. It is evident that the In718 particles are less able

to deform when compared to the Ni particles, due to their reduced ductility. Additionally, it can be stated that the FR of the Ni powder particles may differ slightly in the two coatings. A possible reason for this could be the micro forging effect of the hard In718 particles, which rebound or consolidate on the composite coating, thus contributing to the further flattening of the Ni splats.

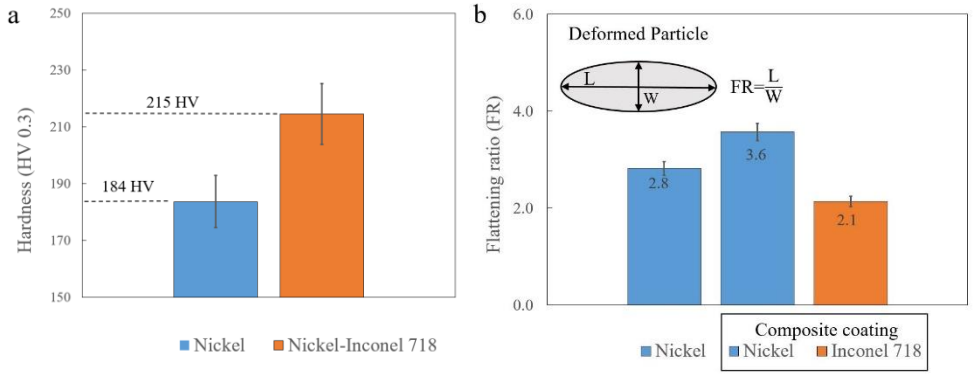

Fig. 10. (a) The microhardness results of the pure Ni and Ni-In718 coatings, (b) flattening ratio of the Ni and In718 particles inside the two coatings.

3.3 Cavitation erosion test

3.3.1 Cavitation erosion resistance

The basic variables used for the evaluation of the cavitation erosion resistance of both the Ni and the Ni-In718 coatings were the mass loss, and the level of degradation (see Fig. 11a and b). It is evident that the superiority of the cold sprayed composite deposit becomes more intense especially between 90-180 min of exposure when its mass loss tends to stabilize while the pure Ni mass loss increases exponentially (Fig. 11a). Hu et al.[13] attributed the low cavitation erosion resistance of Ni to its low hardness and high ductility, which results in ductile fracture of the particles and their subsequent removal. FCC γ phase as observed in Ni and Ni based superalloys is considered to offer improved cavitation erosion resistance when compared to body centered cubic phase, as it exhibits lower strain rate sensitivity[54]. With regards to the incubation period for both coatings, it is difficult to be defined as its accurate determination necessitates the recording of mass loss at shorter time intervals. However, as presented in Fig. 11a, the first detection of mass loss in the case of Ni coating, took place earlier (at 30 min) compared to the composite coating (60 min) which implies a longer incubation period for the latter.

The level of degradation in both coatings increases with increased exposure, with the most significant changes experienced after 120 min of testing. The area affected by the collapse of cavitation bubbles (Fig. 11b) increases in the case of Ni compared to the composite coating, however their magnitude of difference is not correspondingly high compared to the mass loss vs. time diagram. A possible explanation may lie in the fact that the expansion of the composite eroded area during the cavitation erosion testing was not accompanied with a respective increase in the erosion depth.

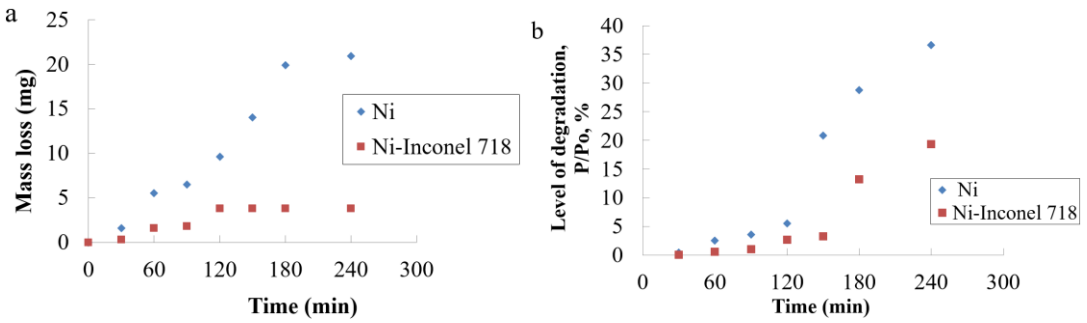

Fig. 11. Comparative cavitation erosion results for Ni and Ni-In718 coatings: (a) mass loss vs. time diagram, (b) level of degradation vs. time diagram.

The relevant literature[3,4,55,56] considers the numerous intrinsic material properties that can affect or be related to the cavitation erosion resistance such as hardness, toughness, ductility and fatigue resistance, tensile strength, work-hardenability and modulus of resilience. However, direct correspondence with a specific property has not yet been reported. With regards to the materials used in the present study, In718 is superior to Ni in all aforementioned properties[57] with the exception of ductility and impact toughness. In addition, stacking fault energy (SFE) is another critical factor which is suggestive that the In718 has superior cavitation erosion resistance when compared to nickel. More specifically, low material SFE is generally accompanied by high cavitation erosion resistance, as it facilitates the formation of planar slips[4] whilst simultaneously impeding the climbing and cross slip processes[58]. In718 is a Ni-based superalloy with a low to medium SFE[36,59] of 50-75 mJ/m^2. As Silgado et al.[58] documented, the addition of iron and chromium (up to 25 wt. %) in Ni-based alloys, results in a reduction in the SFE. In the case of pure Ni, SFE is substantially higher[59], estimated at about 120-130 mJ/m^2.

3.3.2 Morphology of the eroded surfaces

After the termination of the cavitation erosion test (at 240 min), the eroded surfaces were examined using a macroscope as presented in Fig. 12, where the progressive damage of the coating with increasing exposure time is depicted at indicative time intervals. The cavitation erosion attained different characteristics. The mass removal in the case of the Ni coating mainly resulted in the formation of craters with irregular contours (Fig. 12a). However, on the surface of the composite coating, the aforementioned feature was accompanied by the coexistence of intense interparticle microcracks which reveal the particle boundaries (Fig. 12b). It can be assumed that these particles were mainly In718 which protrude intact from the Ni matrix. The repeated bubble collapse seems to cause damage accumulation at two regions, within the particles and at the interparticle boundaries leading to partial and complete particle removal, respectively. However, the existence of In718 in the composite coating appears to impede the second mechanism of mass loss, reducing the sites prone to detachment due to its enhanced cavitation erosion resistance.

a

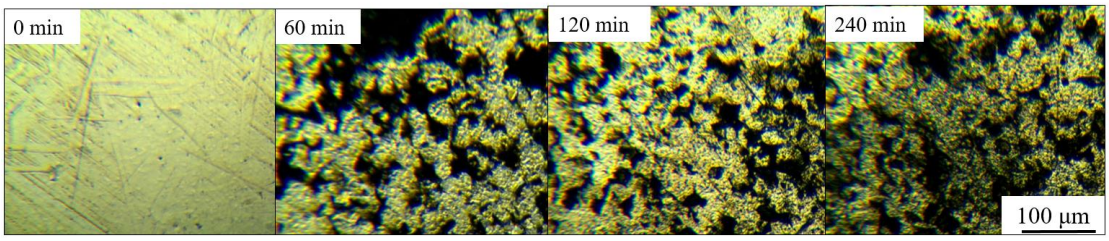

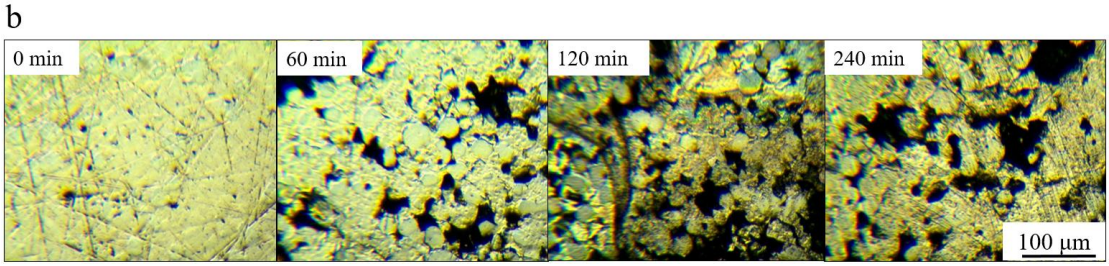

Fig. 12. Macrographs of the eroded surfaces of the two cold sprayed coatings at different testing times: (a) Pure Ni coating, (b) Ni-In718 coating.

The erosion morphology of the coating surfaces was also revealed using SEM as depicted in Fig. 13. The cavities of the Ni coating (Fig. 13a) are dense and not uniformly distributed across the surface. Formation of a single pit may trigger the creation of others in its vicinity, leading to their accumulation at a specific area. Conversely, the composite coating shown in Fig. 13e, presents cavities which are more uniformly dispersed and shallower when compared to the Ni coating presented in Fig. 13b. This outcome reinforces the assumption presented in paragraph 3.3.1, that the mass loss of the Ni coating is mainly attributed to the increases in erosion depth, and lesser to the expansion of the eroded area caused by the formation of new cavitation erosion pits.

The erosion mechanism appears to act more intensively on the interparticle boundaries, as indicated by the red arrows in Fig. 13e, and on the pores, resulting in a full or partial particle removal. The crack propagation was facilitated in the relatively softer Ni coating, where microtunnel formation was also observed due to the action of microjet forces, as indicated with the white arrow in Fig. 13c. In both eroded surfaces, the presence of voids, undulations or wrinkles was not observed, contrary to other relevant investigations of coatings[60] or bulk metals[61,62]. The detachment of particles, as shown in Fig. 13c and f, revealed explicit signs of plastic deformation underneath the removed mass. In the case of the Ni coating, partial particle removal is more intense as indicated by the remains of Ni particles shown by the red arrows in Fig. 13c. Conversely, the erosion cavities of the composite coating attain clearer contours, accompanied by fatigue striations observed in certain areas after the mass removal (black arrows in Fig. 13f) due to the localized cyclic loading and the pressure oscillation. The latter remark complies with the fatigue nature of the cavitation erosion as has been also reported by other researchers[62–64].

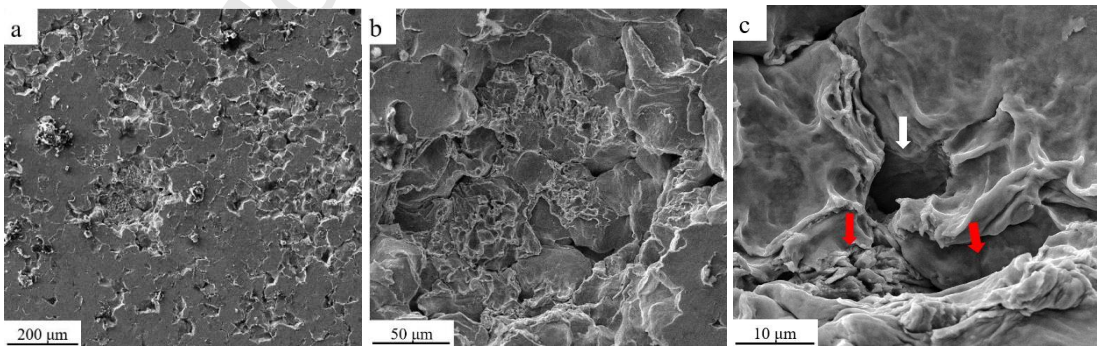

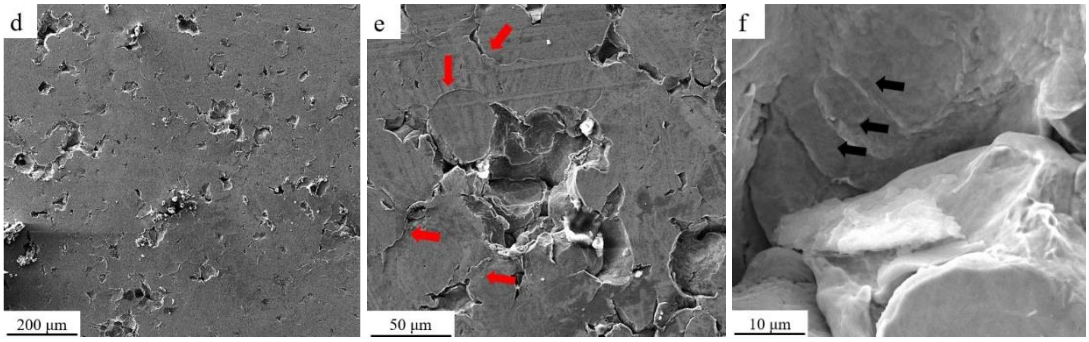

Fig. 13. Electron micrographs (top view) of the eroded surfaces at different magnifications after the end of the cavitation erosion testing (240 min): (a), (b), (c) Ni coating, (d), (e), (f) composite Ni-In718 coating.

The observation cross-sections of the eroded coatings, confirmed the superior cavitation erosion resistance of the composite coating, as a result of the beneficial effect of In718 addition (see Fig. 14), validating the aforementioned remarks. More specifically, nickel particles present partial detachment when exposed to cavitation erosion (red arrows in Fig. 14), acting as favorable sites towards microtunnel (white arrows in Fig. 14a, c, d) and crater formation (white arrow in Fig. 14b). On the contrary, In718 particles (black arrows in Fig. 14c, d) are observed to retain an intact contour. As a result, the predominant mechanism of their removal involves the weakening of the surrounding matrix until the final In718 detachment, similarly to the erosion progress in metal-ceramic composites[13,55].

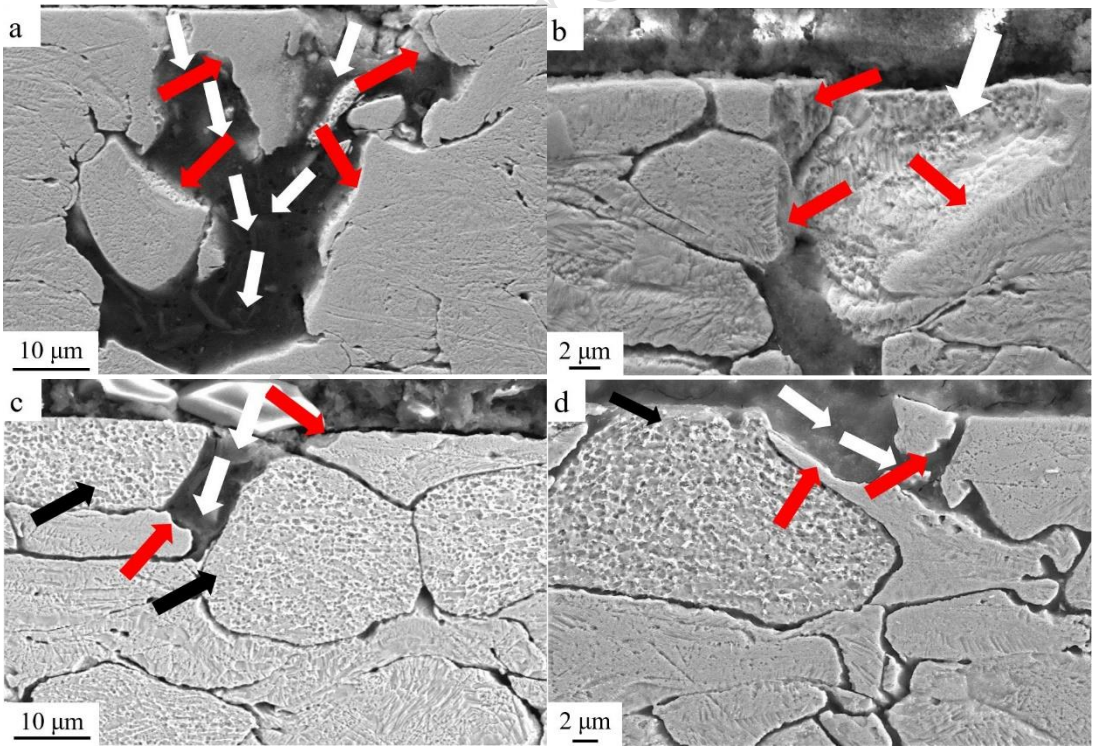

Fig. 14. Electron micrographs (cross-section) of the eroded surfaces at different magnifications after the end of the cavitation erosion testing (240 min): (a), (b), Ni coating, (c), (d), composite Ni-In718 coating.

4. Conclusions

The present study addressed the enhancement of the cavitation resistance of Ni cold sprayed coatings with the addition of In718 powder. Composite coatings were successfully

deposited onto the stainless steel substrates, using nitrogen as the propellant gas instead of helium. The cold spray technique employed in this study exhibited an ample recovery of the reinforcing In718 particles in the Ni matrix, and a moderate increment of the hardness. The composite coating, despite its higher porosity, demonstrated significantly superior cavitation erosion resistance compared to the pure Ni coating. More specifically, In718 addition reduced the overall mass loss by 80% at the end of the experimentation (240 min). In addition degradation of the surface appearance was also decelerated. This was attributed to the different mechanisms of material removal in each case.

The use of the cold spray technique for the production of metal-metal matrix composite coatings shows potential especially in applications where the corrosion and erosion enhancement is the primary objective. However, further research can focus on the optimisation of the particle size distribution within the matrix and the reinforcing material, as well as the fabrication of composite metallic powders with enhanced deposition efficiency.

5. Acknowledgments

The authors would like to thank Enterprise Ireland (EI) and SchuF Valve Technology GmbH (IP2018 0730) for their financial support, as well as the CRANN Advanced Microscopy Laboratory (AML) of Trinity College Dublin for its assistance in the section of microscopy. This work was also supported by the Ministry of Education, Science and Technological Development of the Republic of Serbia, grant numbers III 45012, TR 33007.

6. References

[1] ASM International, ASM Handbook, Volume 18: Friction Lubrication and Wear Technology, ASM International, 2018.

[2] J. Peters, Assessment of valve failures in the offshore oil & gas sector Prepared by TUV NEL Ltd for the offshore oil & gas sector, HSE Books, 2003.

[3] S. Hanke, A. Fischer, M. Beyer, J. dos Santos, Cavitation erosion of NiAl-bronze layers generated by friction surfacing, Wear. 273 (2011) 32–37. doi:10.1016/j.wear.2011.06.002.

[4] R. Singh, S.K. Tiwari, S.K. Mishra, Cavitation erosion in hydraulic turbine components and mitigation by coatings: Current status and future needs, J. Mater. Eng. Perform. 21 (2012) 1539–1551. doi:10.1007/s11665-011-0051-9.

[5] A. Bandar, Fundamentals of Cold Spray Processing: Evolution and Future Perspectives, in: P. Cavaliere (Ed.), Cold Spray Coatings Recent Trends Futur. Perspect., Springer, 2018: pp. 3–24.

[6] S. Yin, E.J. Ekoi, T.L. Lupton, D.P. Dowling, R. Lupoi, Cold spraying of WC-Co-Ni coatings using porous WC-17Co powders: Formation mechanism, microstructure characterization and tribological performance, Mater. Des. 126 (2017) 305–313. doi:10.1016/j.matdes.2017.04.040.

[7] W. Sun, A. Wei, Y. Tan, A. Bhowmik, I. Marinescu, X. Song, W. Zhai, Deposition characteristics of cold sprayed Inconel 718 particles on Inconel 718 substrates with different surface conditions, Mater. Sci. Eng. A. 720 (2018) 75–84. doi:10.1016/j.msea.2018.02.059.

[8] J. Karthikeyan, ASB, The advantages and disadvantages of the cold spray coating process, in: V.K. Champagne (Ed.), Cold Spray Mater. Depos. Process Fundam. Appl., Woodhead Publishing and Maney Publishing, 2007.

[9] S. Alidokht, P. Vo, S. Yue, R.R. Chromik, Erosive wear behavior of Cold-Sprayed Ni-

WC composite coating, Wear. 376–377 (2017) 566–577. doi:10.1016/j.wear.2017.01.052.
[10] S.A. Alidokht, P. Vo, S. Yue, R. Chromik, Cold Spray Deposition of Ni and WC-Reinforced Ni Matrix Composite Coatings, J. Therm. Spray Technol. 26 (2017) 1908–1921. doi:10.1007/s11666-017-0636-4.
[11] Y. Wang, B. Normand, N. Mary, M. Yu, H. Liao, Microstructure and corrosion behavior of cold sprayed SiCp / Al 5056 composite coatings, Surf. Coat. Technol. 251 (2014) 264–275. doi:10.1016/j.surfcoat.2014.04.036.
[12] X. Suo, S. Yin, H. Li, R. Lupoi, Numerical and Experimental Investigation on Bonding Behavior of Cold Sprayed Porous WC-17Co Particles onto Different Substrates, (2018). doi:10.3390/coatings8100367.
[13] H.X. Hu, S.L. Jiang, Y.S. Tao, T.Y. Xiong, Y.G. Zheng, Cavitation erosion and jet impingement erosion mechanism of cold sprayed Ni-Al2O3 coating, Nucl. Eng. Des. 241 (2011) 4929–4937. doi:10.1016/j.nucengdes.2011.09.038.
[14] R. Fernandez, B. Jodoin, Cold Spray Aluminum–Alumina Cermet Coatings: Effect of Alumina Morphology, J. Therm. Spray Technol. 28 (2019) 737–755. doi:10.1007/s11666-019-00845-5.
[15] T.B. Torgerson, M.D. Harris, S.A. Alidokht, T.W. Scharf, S.M. Aouadi, R.R. Chromik, J.S. Zabinski, A.A. Voevodin, Room and elevated temperature sliding wear behavior of cold sprayed Ni-WC composite coatings, Surf. Coatings Technol. 350 (2018) 136–145. doi:10.1016/j.surfcoat.2018.05.090.
[16] F. Li, G. Chang, A. Guosheng, L. Wensheng, C. Jirong, G. Goransky, V. Vaganov, The influence of alumina content in Cu-Al2O3 powder on the properties of cold spraying coating, Adv. Eng. Res. 113 (2016) 782–789. doi:10.4334/jkci.2016.28.2.205.
[17] T.M. Borkar, Processing and characterization of nickel-carbon base metal matrix composites, University of North Texas, 2002.
[18] S. Shin, S. Yoon, Y. Kim, C. Lee, Effect of particle parameters on the deposition characteristics of a hard/soft-particles composite in kinetic spraying, Surf. Coatings Technol. 201 (2006) 3457–3461. doi:10.1016/j.surfcoat.2006.07.255.
[19] M. Yu, M.Y. Ding, H. Ma, H.L. Liao, Microstructure and Corrosion Behavior of Cold-Sprayed Aluminum Alloy/Inconel Composite Coatings, J. Therm. Spray Technol. 28 (2019) 460–471. doi:10.1007/s11666-018-0817-9.
[20] S. Yin, R. Lupoi, Property Enhancement of Cold Sprayed Al-diamond MMC Coating by using Core-shelled Diamond reinforcements, in: ITSC 2019, New Waves Therm. Spray Technol., Yokohama, 2019: pp. 467–475.
[21] W. Wong, E. Irissou, J. Legoux, F. Bernier, Cold Spray Forming Inconel 718, in: Proc. from Int. Therm. Spray Conf. Expo., ASM International, Houston, 2012: pp. 243–248.
[22] R. Singh, K. Rauwald, E. Wessel, G. Mauer, S. Schruefer, A. Barth, S. Wilson, R. Vassen, Effects of substrate roughness and spray-angle on deposition behavior of cold-sprayed Inconel 718, Surf. Coat. Technol. 319 (2017) 249–259. doi:10.1016/j.surfcoat.2017.03.072.
[23] T.S. Sidhu, S. Prakash, R.D. Agrawal, R. Bhagat, Erosion-corrosion behaviour of Ni-based superalloy Superni-75 in the real service environment of the boiler, Sadhana - Acad. Proc. Eng. Sci. 34 (2009) 299–307. doi:10.1007/s12046-009-0009-x.
[24] M.J. Donachie, S.J. Donachie, Superalloys a technical Guide, 2002.
[25] X. Wang, B. Zhang, J. Lv, S. Yin, Investigation on the Clogging Behavior and Additional Wall Cooling for the Axial-Injection Cold Spray Nozzle, J. Therm. Spray Technol. 24 (2015) 696–701. doi:10.1007/s11666-015-0227-1.
[26] S.S. Kalsi, Cold spray coating: an emerging spray technology, Int. J. Latest Trends Eng. Technol. Spec. Issue AFTMME-2017. (2017) 188–192.
[27] D. Srinivasan, V. Chandrasekhar, R. Amuthan, Y.C. Lau, E. Calla, Characterization of Cold-Sprayed IN625 and NiCr Coatings, J. Therm. Spray Technol. 25 (2016) 725–744. doi:10.1007/s11666-016-0382-z.
[28] S. Yin, R. Jenkins, M. Kazasidis, R. Lupoi, Hybrid additive manufacture of 316L

stainless steel with cold spray and selective laser melting : microstructure , mechanical properties and case study, in: ITSC 2019, Yokohama, n.d.: pp. 19–22.
[29] D. Levasseur, S. Yue, M. Brochu, Pressureless sintering of cold sprayed Inconel 718 deposit, Mater. Sci. Eng. A. 556 (2012) 343–350. doi:10.1016/j.msea.2012.06.097.
[30] W. Ma, Y. Xie, C. Chen, H. Fukanuma, J. Wang, Z. Ren, R. Huang, Microstructural and mechanical properties of high-performance Inconel 718 alloy by cold spraying, J. Alloys Compd. 792 (2019) 456–467. doi:10.1016/j.jallcom.2019.04.045.
[31] D. Srinivasan, Cold Spray—Advanced Characterization, in: M. Kay, J. Karthikeyan (Eds.), High Press. Cold Spray-Principles Appl., ASM International, 2016.
[32] M. Calandri, S. Yin, B. Aldwell, F. Calignano, R. Lupoi, Texture and Microstructural Features at Different Length Scales in Inconel 718 Produced by Selective Laser Melting, Materials (Basel). 3 (2019).
[33] S. Ghosh, S. Yadav, G. Das, Study of standard heat treatment on mechanical properties of Inconel 718 using ball indentation technique, Mater. Lett. 62 (2008) 2619–2622. doi:10.1016/j.matlet.2008.01.001.
[34] P.J.P. Kañetas, L.A.R. Osorio, M.P.G. Mata, M.D. La Garza, V.P. López, Influence of the Delta Phase in the Microstructure of the Inconel 718 subjected to "Delta-processing" Heat Treatment and Hot Deformed, Procedia Mater. Sci. 8 (2015) 1160–1165. doi:10.1016/j.mspro.2015.04.180.
[35] R. Konečná, L. Kunz, G. Nicoletto, A. Bača, Fatigue crack growth behavior of Inconel 718 produced by selective laser melting, Frat. Ed Integrita Strutt. 10 (2016) 31–40. doi:10.3221/IGF-ESIS.36.04.
[36] R. Gujrati, C. Gupta, J.S. Jha, S. Mishra, A. Alankar, Understanding activation energy of dynamic recrystallization in Inconel 718, Mater. Sci. Eng. A. 744 (2019) 638–651. doi:10.1016/j.msea.2018.12.008.
[37] M. Sundararaman, N. Sachin, B.S. Jung, V. Amit, P. Bhaskar, R. Kishore, Evolution of Delta Phase Microstructure in Alloy 718, in: 7th Int. Symp. Superalloy 718 Deriv., 2010: pp. 737–750. doi:10.7449/2010/superalloys_2010_737_750.
[38] F.R. Caliari, N.M. Guimarães, D. Aparecida, P. Reis, A.A. Couto, C.D.M. Neto, K. Cristiane, G. Candioto, Study of the Secondary Phases in Inconel 718 Aged Superalloy Using Thermodynamics Modeling, 553 (2013) 23–28. doi:10.4028/www.scientific.net/KEM.553.23.
[39] S.G.K. Manikandan, D. Sivakumar, K. Prasad Rao, M. Kamaraj, Laves phase in alloy 718 fusion zone - Microscopic and calorimetric studies, Mater. Charact. 100 (2015) 192–206. doi:10.1016/j.matchar.2014.11.035.
[40] X. Li, J. Zhang, Q. Fu, E. Akiyama, X. Song, Y. Wang, Q. Li, N. Zou, Tensile mechanical properties and fracture behaviors of nickel-based superalloy 718 in the presence of hydrogen, Int. J. Hydrogen Energy. 43 (2018) 20118–20132. doi:10.1016/j.ijhydene.2018.08.179.
[41] S. Azadian, L.Y. Wei, R. Warren, Delta phase precipitation in inconel 718, Mater. Charact. 53 (2004) 7–16. doi:10.1016/j.matchar.2004.07.004.
[42] M. Jambor, O. Bok, F. Nový, L. Trško, J. Belan, Phase Transformations in Nickel base Superalloy Inconel 718 during Cyclic Loading at High Temperature, Prod. Eng. Arch. 15 (2017) 2013–2016.
[43] Z. Baicheng, X. Mingzhen, T.Y. Teck, W. Jun, W. Pei, Pitting corrosion of SLM Inconel 718 sample under surface and heat treatments, Appl. Surf. Sci. (2019). doi:10.1016/j.apsusc.2019.06.043.
[44] ASTM E407: Standard Practice for Microetching Metals and Alloys, 2015.
[45] ASTM G32: Standard Test Method for Cavitation Erosion Using Vibratory Apparatus, 2016.
[46] S. Holland, X. Wang, J. Chen, W. Cai, F. Yan, L. Li, Multiscale characterization of microstructures and mechanical properties of Inconel 718 fabricated by selective laser melting, J. Alloys Compd. 784 (2019) 182–194. doi:10.1016/j.jallcom.2018.12.380.
[47] S.S. Prabu, K.D. Ramkumar, N. Arivazhagan, Microstructural evolution and precipitation behavior in heat affected zone of Inconel 625 and AISI 904L dissimilar

welds, IOP Conf. Ser. Mater. Sci. Eng. 263 (2017). doi:10.1088/1757-899X/263/6/062073.

[48] M. Godec, D.A. Balantič Skobir, Coarsening behaviour of M23C6 carbides in creep-resistant steel exposed to high temperatures, Sci. Rep. (2016).

[49] W. Li, C. Zhang, H. Liao, J. Li, C. Coddet, Characterizations of cold-sprayed Nickel – Alumina composite coating with relatively large Nickel-coated Alumina powder, 202 (2008) 4855–4860. doi:10.1016/j.surfcoat.2008.04.076.

[50] D. Wolfe, T. Eden, Cold spray particle deposition for improved wear resistance, in: V.K. Champagne (Ed.), Cold Spray Mater. Depos. Process Fundam. Appl., Woodhead Publishing and Maney Publishing, 2007: pp. 264–298.

[51] X.T. Luo, M.L. Yao, N. Ma, M. Takahashi, C.J. Li, Deposition behavior, microstructure and mechanical properties of an in-situ micro-forging assisted cold spray enabled additively manufactured Inconel 718 alloy, Mater. Des. 155 (2018) 384–395. doi:10.1016/j.matdes.2018.06.024.

[52] B. Al-Mangour, R. Mongrain, E. Irissou, S. Yue, Improving the strength and corrosion resistance of 316L stainless steel for biomedical applications using cold spray, Surf. Coatings Technol. 216 (2013) 297–307. doi:10.1016/j.surfcoat.2012.11.061.

[53] T. Novoselova, P. Fox, R. Morgan, W. O'Neill, Experimental study of titanium/aluminium deposits produced by cold gas dynamic spray, Surf. Coatings Technol. 200 (2006) 2775–2783. doi:10.1016/j.surfcoat.2004.10.133.

[54] W. Liu, Y.G. Zheng, C.S. Liu, Z.M. Yao, W. Ke, Cavitation erosion behavior of Cr-Mn-N stainless steels in comparison with 0Cr13Ni5Mo stainless steel, Wear. 254 (2003) 713–722. doi:10.1016/S0043-1648(03)00128-5.

[55] R.K. Kumar, M. Kamaraj, S. Seetharamu, T. Pramod, P. Sampathkumaran, Effect of Spray Particle Velocity on Cavitation Erosion Resistance Characteristics of HVOF and HVAF Processed 86WC-10Co4Cr Hydro Turbine Coatings, J. Therm. Spray Technol. 25 (2016) 1217–1230. doi:10.1007/s11666-016-0427-3.

[56] S. Krebs, F. Gaertner, T. Klassen, Cold spraying of Cu-Al-Bronze for cavitation protection in marine environments, Materwiss. Werksttech. 45 (2014) 708–716. doi:10.1002/mawe.201400307.

[57] ASM International, ASM Handbook, Volume 20: Materials selection and design, 2018.

[58] J. Unfried-Silgado, L. Wu, F. Furlan Ferreira, C. Mario Garzón, A.J. Ramírez, Stacking fault energy measurements in solid solution strengthened Ni-Cr-Fe alloys using synchrotron radiation, Mater. Sci. Eng. A. 558 (2012) 70–75. doi:10.1016/j.msea.2012.07.072.

[59] Z. Tarzimoghadam, D. Ponge, J. Klöwer, D. Raabe, Hydrogen-assisted failure in Ni-based superalloy 718 studied under in situ hydrogen charging: The role of localized deformation in crack propagation, Acta Mater. 128 (2017) 365–374. doi:10.1016/j.actamat.2017.02.059.

[60] E. Qin, B. Wang, Q. Huang, C. Pan, S. Wu, L. Wenli, The cavitation resistance of HVOF deposited WC-CoCr cermet coating in hydraulic application, in: ITSC 2019, New Waves Therm. Spray Technol., Yokohama, 2019.

[61] M. Dojcinovic, O. Eric, D. Rajnovic, L. Sidanin, S. Balos, The morphology of ductile cast iron surface damaged by cavitation, Metall. Mater. Eng. 18 (2012) 165–176.

[62] A. Pola, L. Montesano, M. Tocci, G.M. La Vecchia, Influence of ultrasound treatment on cavitation erosion resistance of AlSi7 alloy, Materials (Basel). 10 (2017). doi:10.3390/ma10030256.

[63] R. Kertscher, J.M. de Moraes, S. Henke, A.N. Allenstein, R.H.G. e Silva, J.C. Dutra, S.F. Brunatto, First Results of Cavitation Erosion Behavior of Plasma Nitrided Niobium: Surface Modification, Mater. Res. 18 (2015) 1242–1250. doi:10.1590/1516-1439.027515.

[64] W. Bedkowski, G. Gasiak, C. Lachowicz, A. Lichtarowicz, T. Łagoda, E. Macha, Relations between cavitation erosion resistance of materials and their fatigue strength under random loading, Wear. 230 (1999) 201–209. doi:10.1016/S0043-

1648(99)00105-2.

Declaration of interests

☒ The authors declare that they have no known competing financial interests or personal relationships that could have appeared to influence the work reported in this paper.

☐The authors declare the following financial interests/personal relationships which may be considered as potential competing interests:

HIGHLIGHTS

- Inconel 718 addition increased the porosity and hardness of the coating
- The cavitation erosion performance was significantly improved
- Inconel 718 offers less sites which may trigger material detachment
- Cavitation erosion revealed a fatigue nature which weakens the metallic bonding